IEEE Access
Multidisciplinary ⋮ Rapid Review ⋮ Open Access Journal

Received April 14, 2020, accepted May 4, 2020, date of publication May 14, 2020, date of current version May 29, 2020.

Digital Object Identifier 10.1109/ACCESS.2020.2994619

Fitness for Service and Reliability of Materials for Manufacturing Components Intended for Demanding Service Conditions in the Petrochemical Industry

ALVARO RODRÍGUEZ-PRIETO[1,2], ANA MARÍA CAMACHO[1], MANUEL CALLEJAS[2], AND MIGUEL A. SEBASTIÁN[1]

[1]Department of Manufacturing Engineering, Universidad Nacional de Educación a Distancia (UNED), 28040 Madrid, Spain
[2]Industrial Inspection and Technical Assistance, SGS Tecnos, 28042 Madrid, Spain

Corresponding author: Alvaro Rodríguez-Prieto (alvaro.rodriguez@ind.uned.es)

This work was supported in part by the Annual Grants Call of the E.T.S.I. Industriales of UNED through the projects of references under Grant 2020-ICF04/B and Grant 2020-ICF04/D, and in part by the Transfer Contract of Research Results with reference under Grant 2019-CTINV-0068.

ABSTRACT A methodology has been developed to quantitatively assess the suitability of use and fitness for service of candidate materials using a novel approach that includes multiple perspectives. As a case study, a carbon steel pipe has been selected for operation in the petrochemical sector. The materials studied were the following: American Petroleum Institute (API) A25, A, B, X42, X46, X52, X56, X60, X65 and X70, as well as American Society for Testing and Materials (ASTM) A-106 Gr. A, B and C. The developed model combines an analytical multiperspective approach with calculation methods based on recognized prestige standards. In the present study, the following material degradation mechanisms have been considered: generalized corrosion, fracture due to mechanical overload and high-temperature degradation. Several novel analysis elements have been incorporated into this new methodology, such as the concept of a suitability matrix and a fitness for service index. The approach allows construction of a decision diagram, and the best alternatives ordered according to the criteria and restrictions that have arisen from the analysis are obtained. Additionally, from the analysis, a series of service limitations are proposed based on the maximum hours of operation of a component. The materials ASTM A-106 Gr. A, API-A, ASTM A-106 Gr. B and API-B maintain the best balance between properties and show greater reliability versus the probability of failure due to the degradation mechanisms considered in this study. In addition, some use limitations such as critical exposure temperature have been determined for these materials (450 °C for ASTM A-106 Gr. A designation and 440 °C for API-B and ASTM A-106 Gr. B designations) to avoid the harmful effects of high-temperature operation on the material mechanical properties.

INDEX TERMS Fitness for service, high-temperature, performance, reliability, use limitations.

I. INTRODUCTION

Reliability evaluation plays an important role in the design and development of any engineering system [1], [2]. Traditional material research relies on a considerable amount of trial experimental designs, which are time-consuming and costly [3]. In addition, the manufacture and operation of components in real service involves additional time-dependent factors that can influence material performance [4]. The manufacturing and operation fields face various global challenges with the support of emerging information technologies for performing diagnosis and optimization.

The development in recent years of different technologies encompassed in the paradigm of the industrial revolution opens the door to intensive monitoring [5]. Continuous monitoring using modern inspection technologies is essential to ensure correct material performance evaluation.

With information and communications technology and the concept of the Internet of Things interconnecting different devices and controllers and offering added value [6],

The associate editor coordinating the review of this manuscript and approving it for publication was Chi-Tsun Cheng.

numerous opportunities have arisen for different predictions of the behavior of equipment and materials that are currently in service using new techniques of predictive analysis and determination of reliability based on evaluation of data obtained by these new technologies.

Uncertainty stems from the assumption of a future event [7], and to identify and mitigate risks, it is crucial to have as much information as possible about the conditions and state of materials making up certain equipment in real time. Through the massive collection of information, not only is the optimization of existing technologies obtained, but it is also possible to develop innovative solutions that provide enhanced capabilities to existing industries [8].

The advancement of nondestructive testing techniques in recent years and their industrial applications provide reliable and objective information [9]. On the other hand, during the last decade, we have also seen the consolidation of several disruptive technologies, such as the Internet of Things (IoT) and scalable computing (big data), as well as the popularization of advanced data analysis (data science) and other techniques related to artificial intelligence [10].

For the analysis of this information, powerful tools capable of filtering are required to sort and analyze data to provide a methodology to support decision-making, such as those related to the selection of materials and/or behavior in service. In this regard, some recent works have described [11], [12] new systems able to recognize patterns and estimate the damage in various steels from metallographic data.

Recently, the worldwide industry has required a change of approach, moving from corrective maintenance through predictive maintenance and recently addressing prescriptive and prognosis approaches. Therefore, it is undoubtedly useful that new methods of analysis and evaluation of the suitability of materials from a combined approach allow the consideration of various mechanisms of the degradation or failure of materials, which are generalized as atmospheric corrosion, overload-induced fracture and high-temperature degradation.

Therefore, regarding these degradation and failure mechanisms, this paper aims to develop a methodology to quantitatively assess the suitability for service of standardized materials intended for use in applications in the petrochemical industry by employing a novel approach that includes multiple perspectives.

This new approach allows predicting behavior in service and therefore involves optimizing the selection of materials by establishing various limitations of use to identify optimal alternatives from a point of view based on reliability.

II. METHODOLOGY

Reliability is intended to give a measure of the probability of failure of a system [13]. To apply the probability method, considerable quantities of information or experimental data are required to construct precise probability distributions of the random inputs. Unfortunately, in many engineering applications, the experimental data are limited [14].

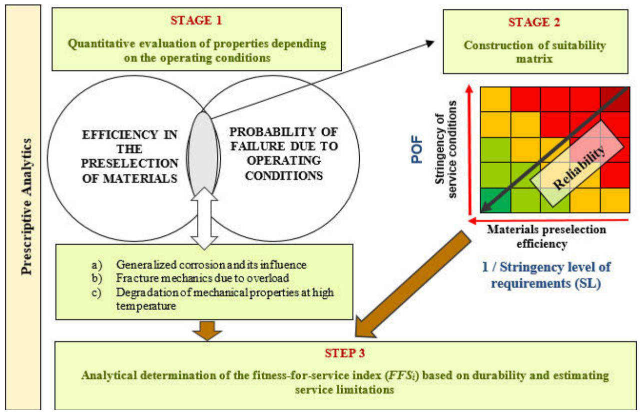

FIGURE 1. Methodology for estimating fitness for service and obtaining reliability and service limitations.

The reliability of a structural system may be estimated at two levels: the component level and the system level [15]. In this work, reliability is centered at the component level. Thus, a decision-making methodology involves considering that when the choice of material is limited to a list of predefined candidates, one difficulty is that the properties of different candidate materials (alternatives) may not indicate any obvious correlation in the given list [16]. Finally, the concept of fitness for service (*FFS*) pertains to the development of quantitative tools to evaluate the ability of existing equipment that experience one or more forms of defects and/or damage to remain in service [17].

The methodology developed in this paper for calculating reliability and fitness for service is a multiperspective approach that combines analysis with calculation methods based on recognized standards such as those issued by the American Petroleum Institute (API). The methodology for calculating the reliability and construction of the suitability matrix is shown in Fig. 1.

The presented methodology has three well-differentiated stages:

- Step 1: An evaluation using a methodology of stringency levels and a multiperspective approach is performed, with different material properties depending on the service conditions. This evaluation considers the following degradation mechanisms:
  1) Generalized corrosion and its influence
  2) Fracture due to overload
  3) Degradation of mechanical properties at high temperature

  In this stage, efficiency is studied in the selection of materials (by using the methodology of stringency levels), and the probability of failure (*POF*) and reliability are determined in terms of the three considered degradation mechanisms.

  Once the analysis considering each of the degradation mechanisms is complete, candidate materials that do not meet the required balance between properties are

TABLE 1. Operating conditions and dimensional parameters used in the calculations.

Process variables	
Service temperature range (°C)	60-80 °C (liquid phase) up to 450 °C (steam system)
Fluid pressure, *P* (MPa)	30
Fluid type	Water
pH	3
External conditions	
Ambient temperature (°C)	30
Dimensional characteristics of the tubing in the study	
Outer diameter, ϕ (m)	0.2
Thickness *t* (m)	0.025
Membrane stresses calculated	
Longitudinal component, σ_l (MPa)	60
Transversal component, σ_t (MPa)	120

TABLE 2. Chemical requirements of seamless pipe [18], [19].

Designation of the material	Chemical composition (wt%)					Mechanical properties (MPa)	
	C	Mn	P	S	Ti	σ_Y	σ_U
API-A25 Cl II	0.21	0.60	0.08	0.03	-	172	310
API-A	0.22	0.90	0.03	0.03	-	207	331
API-B	0.28	1.20	0.03	0.03	0.04	241	414
API-X42	0.28	1.30	0.03	0.03	0.04	290	414
API-X46	0.28	1.40	0.03	0.03	0.04	317	434
API-X52	0.28	1.40	0.03	0.03	0.04	359	455
API-X56	0.28	1.40	0.03	0.03	0.04	386	490
API-X60	0.28	1.40	0.03	0.03	0.04	414	517
API-X65	0.28	1.40	0.03	0.03	0.06	448	531
API-X70	0.28	1.40	0.03	0.03	0.06	483	565
ASTM A-106 Gr. A	0.25	0.93	0.035	0.035	-	205	330
ASTM A-106 Gr. B	0.30	1.06	0.035	0.035	-	240	415
ASTM A-106 Gr. C	0.35	1.06	0.035	0.035	-	275	485

discarded. This analysis yields some restrictions that are used in step 3.

- Step 2: A suitability matrix in which the materials are classified if they have not been discarded is used in step 2. This step is achieved to evaluate the reliability of materials based on the probability of failure (*POF*) and the efficiency of the preselection of materials.
- Finally, in step 3, the fitness for service index is calculated for candidate materials using an analytical approach to obtain in-service limitations depending on the operating hours (durability) expected by design.

Once the methodology is described, a case study is presented: carbon steel pipe intended for operation in the petrochemical industry. The service conditions defined in the case study are given in Table 1.

The materials selected for study as candidates for the manufacture of pipes intended for petrochemical industry plants are given in Table 2 along with their most important properties.

Regarding the chemical properties, as shown in Table 2, the carbon and manganese contents exhibit the most significant differences among the various materials; these elements greatly influence the mechanical properties, such as the yield stress (σ_y) and maximum tensile strength (σ_U). Thus, increasing the contents of carbon and manganese increases these parameters.

TABLE 3. Mechanisms of degradation and failure.

Mechanism of degradation/ failure	Description	Associated damage	Basic parameters for analysis
Generalized corrosion	Generalized external corrosion. Reaction kinetics influenced by the ambient humidity, the presence of Cl^- and temperature.	Loss of thickness above a certain threshold, may trigger the loss of mechanical integrity and break the component.	pH and operating temperature range.
Fracture due to overload	Break under stress applied below its maximum strength. Under extreme loading conditions, the materials experience permanent deformations where they pass the elastic zone [20-21].	Catastrophic failure involving economic, environmental and personal injury consequences.	Yield point (σ_Y) Ultimate tensile strength (σ_U).
High-temperature degradation	High-temperature degradation where plastic deformation occurs in the metal when subjected to stresses below normal resistance.	Degradation of mechanical properties that can cause failure with economic, environmental and personal injury consequences.	Maximum allowable stress variation as a function of the temperature.

The following degradation mechanisms were selected for evaluation: general corrosion, fracture due to mechanical overload and high-temperature degradation (Table 3).

Based on the analysis of the considered degradation and failure mechanisms, Step 1 is developed according to the methodology outlined in Fig. 1 as follows.

A. STEP 1. QUANTITATIVE EVALUATION OF PROPERTIES DEPENDING ON THE OPERATING CONDITIONS

Mechanical loading, geometric size, material properties, service conditions and environmental effects such as atmospheric corrosion are heterogeneous and time-variant. Thus, material properties may decay over time and can be presented as degradation mechanisms [22].

The evaluation of the properties of materials depending on the service conditions is a complex task that must be approached from multiple perspectives. Only this type of approach allows optimization of the combination of strength and ductility properties with a suitable profile calculation, which allows selection of an appropriate thickness that will provide component structural integrity and that is sufficient to

TABLE 4. Calculation of the ratio between the yield strength and maximum strength (σ_Y/σ_U), the maximum elongation at fracture (e %), the stress to collapse (σ_{col}) and the safety factor (*SF*) for each of the materials according to the maximum applied membrane stress (σ_t).

Grade	σ_Y/σ_U	*e* (%)	σ_{col} (MPa)	*SF*
A25Cl. II	0.55	5.96	241.00	0.31
A	0.63	5.11	269.00	0.37
B	0.58	4.66	327.50	0.41
X42	0.70	3.94	352.00	0.45
X46	0.73	3.68	375.50	0.47
X52	0.79	3.32	407.00	0.49
X56	0.79	3.15	438.00	0.50
X60	0.80	2.99	465.50	0.52
X65	0.84	2.80	489.50	0.53
X70	0.85	2.65	524.00	0.54
A-106 Gr. A	0.62	5.15	267.50	0.37
A-106 Gr. B	0.58	4.68	327.50	0.41
A-106 Gr. C	0.57	4.27	380.00	0.44

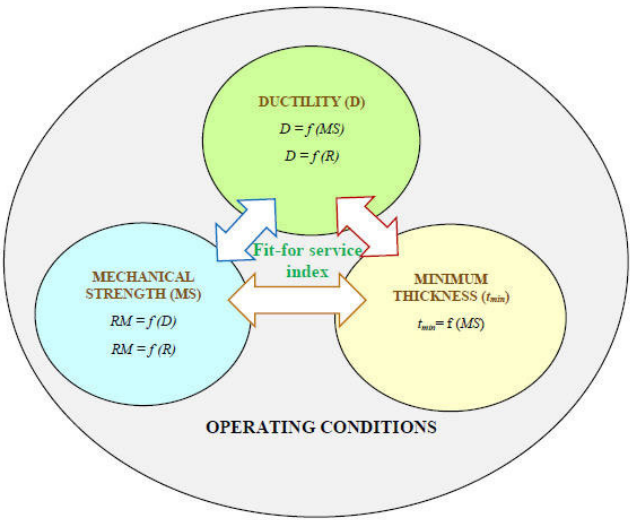

FIGURE 2. Balance among strength, ductility and minimum thickness.

palliate possible loss of corrosion thickness over an extended period of operation (Fig. 2).

In general, maximizing the mechanical strength involves reducing the ductility and vice versa. Therefore, it is necessary to find an optimal balance between mechanical strength and ductility. On the other hand, greater strength means reducing the resulting thickness. However, the thickness can also be increased by design considering external factors such as generalized corrosion. As is clearly well known, adequate strength with adequate ductility is essential to prevent brittle behavior [23].

Finding a balance among these three parameters (strength, ductility and minimum thickness) requires modeling to calculate the fitness for service index from the concepts of probability of failure (*POF*) and reliability (*R*) calculated in steps 2 and 3 of the methodology.

For evaluation of the mechanical strength depending on the mechanical stresses considered (Table 1), the ratio between the maximum tensile strength (σ_U) and yield strength (σ_Y) is

TABLE 5. Correspondence between quantitative and qualitative stringency scale levels.

Stringency levels (Quantitative)	Qualitative correspondence with stringency level
1	Insufficient
2	Mild
3	Medium
4	Moderate
5	High (SL_{max})

calculated. Additionally, the maximum elongation at fracture ($e\%$) according to API 5L (2018), the effort to collapse (σ_{col}) and the structural safety factor (*SF*) are calculated according to Eqs. 1 to 3, respectively.

$$e = 1.944 \frac{\sigma\gamma^{0.2}}{UTS^{0.9}} \quad (1)$$

$$\sigma = \frac{\sigma\gamma + UTS}{2} \quad (2)$$

$$SF = \frac{\sigma_t}{\sigma_\gamma} \quad (3)$$

Table 4 shows the parameters calculated using Eqs. 1 to 3.

The chemical and mechanical properties indicated in Tables 2 and 4 are evaluated using an analysis by stringency levels divided into five scales, as indicated in Table 5.

The methodology for assigning *SL* to different technological requirements has been developed depending on the type of requirement and considerations taken into account in its analysis [2], [24].

Eqs. 4 and 5 show the allocation methodology. $SL = 5.00$ is assigned to the requirement of greater value (Eq. 4):

$$SL = 5.00 \ \ \forall \max\{L_e(\text{API, ASTM})\}. \quad (4)$$

Eq. 5 is used to calculate *SL* of the remaining requirements for the other materials analyzed:

$$SL = \frac{L_{e,min}}{L_e} SL_{Max} \quad (5)$$

where L_e corresponds to the value of the requirement to be analyzed from all {API, ASTM} and $L_{e,min}$ is the minimum value of the set.

The results of applying Eqs. 4 and 5 are presented in Table 6, wherein SL_S refers to the average stringency levels obtained for the ratio (σ_Y/σ_U), collapse stress (σ_{col}) and structural safety factor (*SF*) and SL_e defines the material ductility from the analysis of the condition of maximum elongation at fracture.

Fig. 3 shows the decrease in the requirement of elongation dependent on an increase in the strength characteristics, allowing the first constraint or boundary condition to be obtained to find a balance between the strength and ductility of the material.

Given the inverse relationship between the requirements of mechanical strength and ductility, to find a balance between

TABLE 6. Stringency levels for parameters σ_Y/σ_U, σ_{col}, and *SF* and mean stringency levels of mechanical requirements (SL_S) and ductility requirements (SL_e).

Grade designation	$SL(\sigma_Y/\sigma_U)$	SL (σ_{col})	SL (SF)	SL_S	SL_e
A25	3.25	2.30	2.90	2.82	5.00
A	3.66	2.57	3.45	3.23	4.29
B	3.40	3.13	3.84	3.46	3.91
X42	4.10	3.36	4.23	3.89	3.31
X46	4.27	3.58	4.39	4.08	3.08
X52	4.61	3.88	4.60	4.37	2.78
X56	4.61	4.18	4.71	4.50	2.65
X60	4.68	4.44	4.81	4.64	2.51
X65	4.93	4.67	4.91	4.84	2.35
X70	5.00	5.00	5.00	5.00	2.23
A-106 Gr. A	3.63	2.55	3.43	3.20	4.32
A-106 Gr. B	3.38	3.13	3.83	3.44	3.93
A-106 Gr. C	3.32	3.63	4.12	3.69	3.58

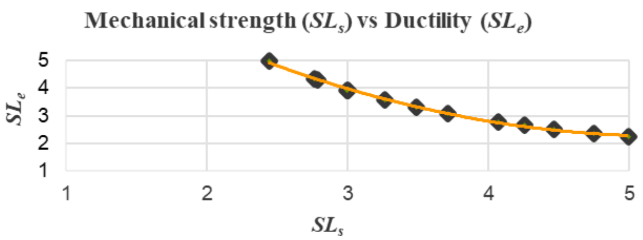

FIGURE 3. Representation of the calculated SL_S (mechanical strength) versus SL_e (ductility).

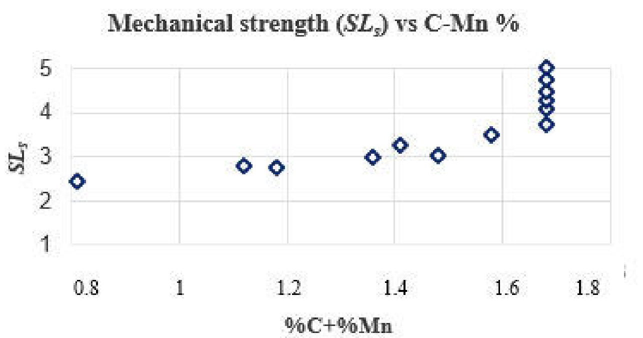

FIGURE 4. SL_S (mechanical strength) dependent on the wt% content of C and Mn.

the two groups of characteristics, the equilibrium restriction designated as Constraint 1 is defined as follows:

$$\textbf{Constraint1}: 3 < SL_S, \quad SL_e < 4$$

Following the resolution of the balance in Fig. 2, where the relationship among the strength, ductility and minimum thickness of materials is shown, the ideal combination of chemical composition (C% + Mn%) is determined. The values of SL_S (Fig. 4) and SL_e (Fig. 5) are shown versus the percentage content (mass) of carbon and manganese.

According to the relationship between chemical composition and mechanical properties, to define a balance between strength and ductility, Constraint 2 must be imposed.

$$\textbf{Constraint2}: \%C + \%Mn = 1.4(\pm 10\%) = 1.26 - 1.54$$

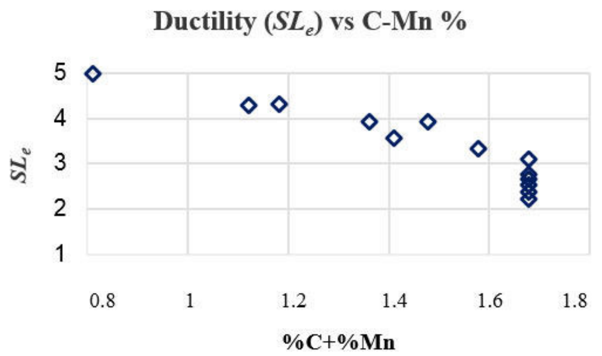

FIGURE 5. SL_e (ductility) dependent on the wt% content of C and Mn.

After preliminary analysis of the properties of the materials, we proceed to study the influence of the material properties on the susceptibility to the degradation mechanisms considered in this work. According to the degradation mechanisms shown in Table 3, the properties of the materials are analyzed, starting with an evaluation of the corrosion resistance of each designation of standard material and its influence on the mechanical integrity of the component (a). We then study fracture due to overload (b) by cumulatively considering the loss of integrity due to corrosion. Finally, in subsection (c), an evaluation of susceptibility to high-temperature degradation is carried out.

1) EVALUATION OF RESISTANCE TO GENERAL CORROSION AND INFLUENCE ON THE MECHANICAL INTEGRITY

By using various standards, such as API RP 581 [25] and ISO 9223 [26], in this section, various estimates are carried out that allow later analysis for predictively evaluating the corrosion resistance of the materials under study and determining how this mechanism of degradation affects the mechanical integrity of the component.

Table 7 shows the estimated corrosion rate for the first year of exposure for API RP 581 [25]. The corrosion rate is calculated for the first year of exposure, where R_{corr} = 3.81 mm/year, interpolated to pH = 3 and 79 °C.

The corrosion rate estimated for the first year of exposure (R_{corr}) in Table 8 can be used to classify the sample into the category of C2 according to the defined scale in the ISO 9223 [26] standard.

For corrosivity category C2, we can estimate the thickness loss after the first year of exposure according to the estimates provided by the ISO 9224 [27] standard. In Table 9, the loss of thickness (Δt) is shown in μm depending on the exposure time T_{exp}).

The corrosion rate can be calculated according to the calculation method described in API 570 [28] using Eq. 6.

$$v_{corr} = \frac{\Delta t}{\Delta T_{exp}} \tag{6}$$

Thus, as estimated by API 581 [25] for corrosion from the first year (Table 7) and for durability of at least 100,000 h (11.41 years), a loss of thickness from corrosion of 4.66 mm

TABLE 7. Determination of the corrosion rate (mm/year) for the first year of exposure, depending on the PH and temperature (carbon steel), according to API RP 581 [25].

pH	Temperature (°C)			
	38	52	79	93
0.5	25.37	25.37	25.37	25.37
0.80	22.86	25.37	25.37	25.37
1.25	10.16	25.37	25.37	25.37
1.75	5.08	17.78	25.37	25.37
2.25	2.54	7.62	10.16	14.22
2.75	1.52	3.30	5.08	7.11
3.25	1.02	1.78	2.54	3.56
3.75	0.76	1.27	2.29	3.18
4.25	0.51	1.02	1.78	2.54
4.75	0.25	0.76	1.27	1.78
5.25	0.18	0.51	0.76	1.02
5.75	0.10	0.38	0.51	0.76
6.25	0.08	0.25	0.38	0.51
6.80	0.05	0.13	0.18	0.25

TABLE 8. Corrosion rate after the first year of exposure (R_{corr}) in micrometers/year for different categories of corrosion according to ISO 9223 [26].

Corrosivity category	Corrosion rate after the first year of exposure (R_{corr}) in μm/year
C1	$R_{corr} \leq 1.3$
C2	$1.3 < R_{corr} \leq 16$
C3	$16 < R_{corr} \leq 50$
C4	$50 < R_{corr} \leq 80$
C5	$80 < R_{corr} \leq 200$
CX	$200 < R_{corr} \leq 700$

TABLE 9. Maximum thickness loss due to corrosion from the first year of exposure [27].

T_{exp} (years)	Δt (μm)
1	1.3
2	1.9
5	3.0
10	4.3
15	5.4
20	6.2

is expected according to the ISO 9224 [27] prediction (shown in Table 9).

2) FRACTURE DUE TO OVERLOAD

The thickness loss due to corrosion should be considered a reduction in the mechanical integrity of the pipe whose minimum thickness is calculated using Eq. 7.

$$t_{min} > \frac{P \cdot R_d}{\sigma_y} \tag{7}$$

However, the limit of thickness before fracture can be calculated by Eq. 8.

$$t_{min\,no\,collapse} = \frac{P \cdot R_d}{\sigma_{col}} \tag{8}$$

TABLE 10. Calculated minimum thickness to prevent plastic deformation (t_{min}) and fracture ($t_{min\,no\,collapse}$) and critical time to collapse ($T_{critic\,collapse}$).

Material	t_{min} (mm)	$t_{min,\,corr}$ (mm) *	$t_{min\,no\,collapse}$ (mm)	$\sigma_{t,\,corr}$ (MPa)	$T_{critic\,collapse}$ (years)
A25	26.43	21.77	12,45	68.91	11.78
A	21.96	17,30	11.15	86.71	8.84
B	18.86	14.20	9.16	105.63	8.08
X42	15.67	11.01	8.52	136.19	5,65
X46	14.34	9.68	7,99	154.98	4.94
X52	12.66	8.00	7.37	187.47	3.99
X56	11.78	7.12	6.85	210.80	3.72
X60	10.98	6.32	6.44	237.37	3.40
X65	10.15	5.49	6,13	273.42	2.94
X70	9.41	4.75	5.73	315.73	2.67
A-106 Gr. A	22.17	17.51	11.21	85.65	8.98
A-106 Gr. B	18.94	14.28	9.16	105.05	8.16
A-106 Gr. C	16.53	11.87	7.89	126.38	7.25

Note*: Calculations based on the prediction of thickness loss by corrosion to API 581 (Table 7).

Thus, Eq. 9 can be used to determine the time that elapses from the start of plastic deformation ($T_{critic,collapse}$) as follows:

$$t_{critic\,collapse} = \frac{t_{min} - t_{\min no\,collapse}}{v_{corr} + R_{corr}} \tag{9}$$

where V_{corr} is the corrosion rate after the first year of exposure.

Table 10 shows the minimum thickness (t_{min}), the minimum thickness after corrosion loss ($t_{min,corr}$), the thickness limit before collapse ($t_{min\,no\,collapse}$) and the maximum allowable membrane stress considering reduced thickness by corrosion ($\sigma_{t,corr}$).

Calculations made after loss of corrosion thickness allow the verification of how the resulting thickness (arising from the selection of the material) is essential to alleviate the possible effects of thickness loss due to widespread corrosion phenomena. This analysis allows assessment of whether it is worth employing a material with better mechanical resistance (at the expense of ductility) and increasing the excess thickness to avoid overstressing fracture after a possible loss of thickness due to corrosion.

For the focus on evaluating candidate materials, Fig. 6 shows a representation of the effect of the thickness loss on membrane stresses after 100,000 h of operation.

At 80 °C, for a calculated corroded thickness of 4.66 mm after 100,000 h of operation at pH = 3 (according to Table 1), materials API A25, A and B as well as materials ASTM A-106 Gr. A and ASTM Gr. B meet the requirement imposed on the maximum recommended value of elastic stress extrapolated at 80 °C for carbon steels according to API STD 530 ($\sigma_{Y,API530,80}$). Eq. 10 shows the calculation of the probability

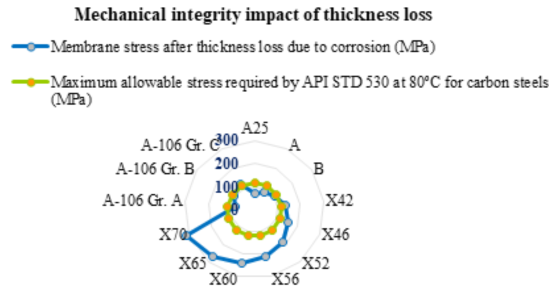

FIGURE 6. Effect of thickness loss due to corrosion after 100,000 h of operation and comparison with the API STD 530 maximum allowable stress.

TABLE 11. $POF_{corr+overload}$ calculations as a function $T_{critic\,scollapse}$.

Material	$T_{critic\ collapse}$ (years)	$POF_{corr+overload}$
API-A25	11.78	0.08
API-A	8.84	0.11
API-B	8.08	0.12
API-X42	5.65	0.18
API-X46	4.94	0.20
ASTM A-106 Gr. A	8.98	0.11
ASTM A-106 Gr. B	8.16	0.12
ASTM A-106 Gr. C	7.25	0.14

of failure (POF) based on the maximum time in operation.

$$POF = \frac{1}{T_{max}} \tag{10}$$

T_{max} = maximum operating time (in hours) depending on the considered degradation mechanisms.

Thus, Table 11 shows the calculation of the probability of failure due to loss of thickness by corrosion and overload ($POF_{corr+overload}$) based on the critical time ($T_{critic,collapse}$) that elapsed between the start of plastic deformation and breakage.

3) EVALUATION OF HIGH-TEMPERATURE STRENGTH

By extrapolating the data representing the relationship between the maximum stress before rupture ($\sigma_{U,max}$) as a function of temperature and the hours of operation foreseen by design (T_{DL}) given in API STD 530 [29], Fig. 7 illustrates that the maximum allowable stress ($\sigma_{U,max}$) decreases slightly faster above approximately 300 °C. Furthermore, we observe that the difference between the maximum allowable stresses ($\sigma_{U,max}$) for 100,000 h and 20,000 h (since they are the extremes of operation hours postulated by API STD 530) increases more rapidly above 400 °C, with a greater difference from 450-500 °C (as shown in Fig. 8). This representation was obtained by extrapolating data from API STD 530 [29] (including estimated life – T_{DL}–, operating temperature – T – and maximum allowable stress – $\sigma_{U,max}$–).

Thus, it is possible to obtain the following constitutive equations, where Eqs. 11 to 14 relate the maximum allowable stress ($\sigma_{Y\,max}$) according to API STD 530 depending on the

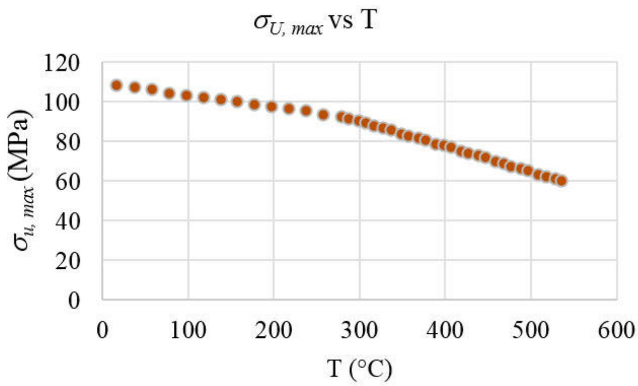

FIGURE 7. Maximum allowable rupture stress as a function of temperature.

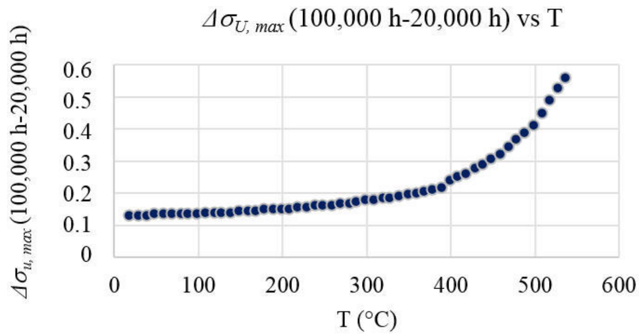

FIGURE 8. Difference in the estimated values of the maximum allowable rupture stresses after 100,000 h and 20,000 h in operation.

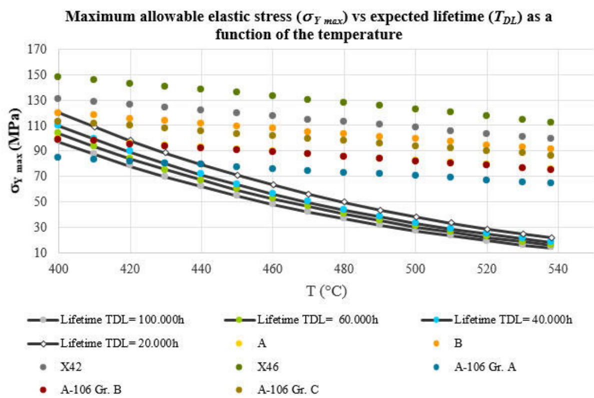

FIGURE 9. Maximum allowable stress ($\sigma_{Y\,max}$) vs. estimated life (T_{DL}) based on the operating temperature.

temperature and estimated life:

$$\sigma_{Y\,max\,(100k\ h)} = 0.0027\,T^2 - 3.1450\,T + 919.29 \tag{11}$$

$$\sigma_{Y\,max\,(60k\ h)} = 0.0028\,T^2 - 3.2354\,T + 952.60 \tag{12}$$

$$\sigma_{Y\,max\,(40k\ h)} = 0.0028\,T^2 - 3.3165\,T + 981.54 \tag{13}$$

$$\sigma_{Y\,max\,(20k\ h)} = 0.0029\,T^2 - -3.4547\,T + 1031.60 \tag{14}$$

By focusing on the temperature range (temperature) where the mechanical properties are more strongly negatively affected (400-500 °C), Fig. 9 shows the maximum elastic

TABLE 12. Color-coded matrix applied to *CET* estimation.

Operating time as designed (T_{DL})	Color code assigned
<20,000 h ∀ $\sigma_{Y,\ max} < \sigma_{Y\ API\ 530}$	
20,000-40,000 ∀ $\sigma_{Y,\ max} < \sigma_{Y\ API\ 530}$	
40,000-60,000 ∀ $\sigma_{Y,\ max} < \sigma_{Y\ API\ 530}$	
60,000-100,000 ∀ $\sigma_{Y,\ max} < \sigma_{Y\ API\ 530}$	
> 100,000 ∀ ∀ $\sigma_{Y,\ max} < \sigma_{Y\ API\ 530}$	

CET (ºC)	API-A	A-106 Gr. A	API-B	A-106 Gr. B	API-X42	A-106 Gr. C	API-X46
400	56.11	55.57	65.33	65.06	78.61	74.54	85.93
410	55.22	54.69	64.29	64.03	77.36	73.36	84.57
420	54.26	53.73	63.17	62.91	76.01	72.08	83.09
430	53.29	52.78	62.05	61.79	74.66	70.80	81.62
440	52.33	51.83	60.93	60.67	73.31	69.52	80.14
450	51.37	50.87	59.80	59.56	71.96	68.24	78.66
460	50,40	49.92	58.68	58.44	70.61	66.96	77.19
470	49.36	48.89	57.47	57.23	69.16	65.58	75.60
480	48.40	47.93	56.35	56.12	67.81	64.30	74.12
490	47.44	46.98	55.23	55,00	66.46	63.02	72.65
500	46.47	46.03	54.11	53.88	65.11	61.74	71.17

FIGURE 10. Matrix for estimating the critical exposure temperature (*CET*) as a function of service hours for the material at that temperature, using criteria exhibited in Table 12.

TABLE 13. Critical exposure temperature (*CET*), time in operation by design at 450 °C ($T_{DL\ T^a}$) and probability of failure due to high-temperature degradation (POF_{T^a}).

Material	CET (°C)	$T_{DL\ T^a}$ (years) ∀ T= 450°C	POF_{T^a}
A	450	11.42	0.09
B	440	6.85	0.15
X42	430	2.28	0.44
X46	410	2.28	0.44
A-106 Gr. A	450	11.42	0.09
A-106 Gr. B	440	6.85	0.15
A-106 Gr. C	420	2.28	0.44

stress ($\sigma_{Y\ max}$) versus the estimated life (T_{DL}) depending on the operating temperature.

After the above analysis, an interpolation of values is performed to obtain the maximum elastic stress ($\sigma_{Y,API\ 530}$) allowed by API STD 530 [29] at 400-500 °C (the temperature range in which the degradation is more accelerated). This analysis allows a comparison of the maximum stresses until rupture ($\sigma_{U,\max}$) calculated for each material with $\sigma_{Y,API\ 530}$. Thus, the critical exposure temperature (*CET*) of each material can be determined.

In Table 12, several color codes are defined for use in the estimation matrix (Fig. 10) for the *CET*).

Table 13 shows the critical exposure temperature (*CET*), time in operation by design (T_{DL}) and probability of failure (*POF*) due to high-temperature degradation (POF_{T^a}).

TABLE 14. Probability of failure associated with corrosion and overload ($POF_{corr+overload}$) and with high-temperature degradation (POF_{T^a}), along with the total probability (POF_{total}), reliability (*R*) and inverse of the mean stringency level of mechanical strength (SL_S) and ductility (SL_E).

Material	$POF_{corr+overload}$	POF_{T^a}	POF_{total}	Reliability (*R*)	$2 / SL_S + SL_e$
A	0.11	0.09	0.20	0.80	0.27
B	0.12	0.15	0.27	0.73	0.27
X42	0.18	0.44	0.62	0.38	0.28
X46	0.20	0.44	0.64	0.36	0.28
A-106 Gr. A	0.11	0.09	0.20	0.80	0.27
A-106 Gr. B	0.12	0.15	0.27	0.73	0.27
A-106 Gr. C	0.14	0.44	0.58	0.42	0.28

B. STEP 2. CONSTRUCTION OF THE SUITABILITY MATRIX

The reliability (*R*) in relation to the probability of failure (*POF*) of a component, equipment or system can be obtained from Eq. 15.

$$R = 1 - POF \tag{15}$$

The focus of this article includes the novel element of the construction of a suitability matrix and the calculation of the fitness for service (FFS_i) index (Fig. 1) of the materials selected for study, which are shown later in this section. The concept of the suitability matrix for reliability is based on the quantification of the probability of failure, and the stringency of the technological requirements of the materials has an important influence on the service performance and service life of components manufactured with these materials. The probability of failure (*POF*) is calculated from Eq. 16.

$$POF = POF_{corr+overload} + POF_{T^{\circ}} \tag{16}$$

Table 14 shows the probability of failure associated with corrosion and overload ($POF_{corr+overload}$) and with high-temperature degradation (POF_{T^a}), together with the total probability (POF_{total}), reliability (*R*) and inverse of the mean value ($2/SL_s + SL_e$) of the stringency levels of mechanical strength (SL_S) and ductility (SL_e).

The data obtained represent the probability of complete failure (POF_{total}) versus reliability (*R*) for each of the candidate materials (Fig. 11).

In addition, the data obtained allow us to build the suitability matrix (Fig. 12).

As shown in Fig. 12, the stringency levels of the requirements used along with *POF* allow us to construct the suitability matrix that defines a relative position that can be used for the elaboration of tailored-made inspection and testing plans for predictive maintenance, allowing us to achieve a reliability target with minimum inspection and manufacturing costs [30], [31]. This analysis shows that the best alternatives are the materials ASTM A-106 Gr. A and API-A (high qualitative reliability) and ASTM A-106 Gr. B and API-B (mean qualitative reliability). Thus, materials API X42 and X46 are discarded at this stage. Low-carbon steels should exhibit ductile behavior [32] balanced with mechanical strength.

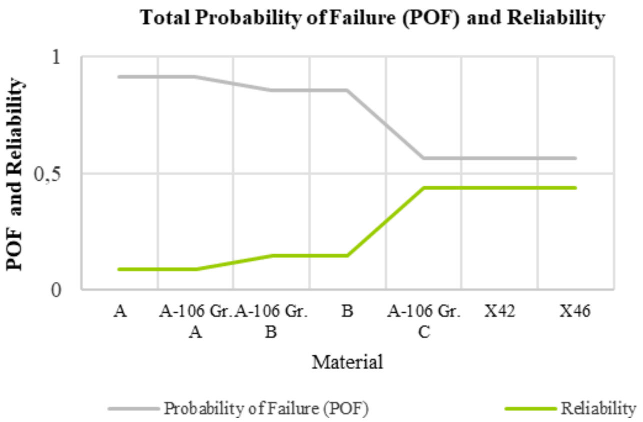

FIGURE 11. Representation of the overall probability of failure (POF_{total}) versus reliability (R) for each of the candidate materials.

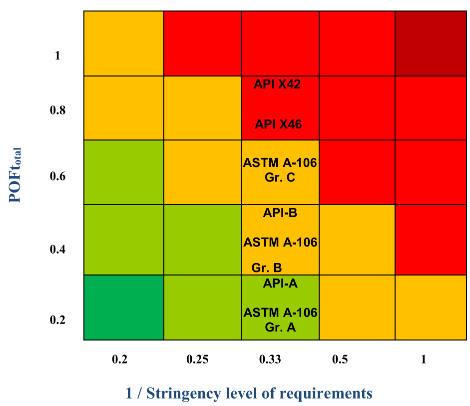

FIGURE 12. Suitability matrix representing POF_{total} versus the inverse of the level of stringency of requirements (mean value calculated for the mechanical strength and ductility).

III. RESULTS

The increasing complexity of engineering systems and their working environments enhances the importance of operational reliability throughout a lifecycle [33], [34].

Therefore, the best alternatives correspond to the standard materials API-A and B and ASTM A-106 Gr. A and Gr. B. A comparative study (Step 3) - in which the durability of the material is included - is performed. Moreover, some limitations in service that arise upon application of the methodology are described.

A. STEP 3. ANALYTICAL DETERMINATION OF THE FITNESS FOR SERVICE INDEX (FFS_i) BASED ON DURABILITY AND ESTIMATION OF SERVICE LIMITATIONS

In step 3, the fitness for service index (FFS_i) for candidate materials (Fig. 13) can be estimated using Eq. 17.

$$FFS_i = SL \cdot R \tag{17}$$

In view of the results, the highest values of FFS_i are obtained for the materials API-A and ASTM A-106 Gr. A. On the other hand, Table 15 shows some restrictions arising from the analysis and defines exclusion parameters to be considered in the analysis.

After determining the candidate materials with better characteristics, upon application of the exclusion criteria, Table 16 defines a series of parameters (and an optimization strategy) for the order of selection of materials that meet the criteria shown in Table 15.

With the results shown in Tables 15 and 16, a selection diagram (Fig. 14) can be made using the main groups of

FIGURE 13. Fitness for service index (FFS_i).

TABLE 15. Exclusion criteria used: parameters to evaluate, restrictions applied and materials that meet the restriction.

Parameter to	Restriction	Materials that meet the
$\sigma_{t,\,corr}$	$\sigma_{t,\,corr} < \sigma_{Y,\,API\ 530,\ 80°C}$	API A25, A and B, ASTM A-106 Gr. A and Gr. B
SL_S	3-4	A, B, X42, X46
SL_e	3-4	A-106 Gr. A, Gr. B and Gr. C
% C +% Mn	1.26-1.54	B, X42, ASTM A-106 Gr. B and Gr. C
Reliability (qualitative)	Green area	A, B, ASTM A-106 Gr. A and Gr. B
Estimated lifetime at *T* = 450 °C	Between 60,000 and 100,000 h	A, B, ASTM A-106 Gr. A and Gr. B

TABLE 16. Selection criteria used: parameters to evaluate, optimization strategies, results and optimal candidates (in order of selection).

Parameter to assess	Optimization strategy	Results	Optimal candidates (in order of selection)
Reliability (*R*)	Max (*R*)	*R (ASTM A-106 Gr. A)* = 0.89 *R (ASTM A-106 Gr. B, API-B)* = 0.83	ASTM A-106 Gr. A > API B = ASTM A-106 Gr. B
Critical exposure temperature (*CET*)	Max (*CET*)	*CET (ASTM A-106 Gr. A)*= 450 °C *CET (ASTM A-106 Gr. B, API-B)*= 440 °C	ASTM A-106 Gr. A> API B = ASTM A-106 Gr. B
Critical time to collapse ($T_{critic,\,collapse}$)	Max ($T_{critic,\,collapse}$)	$T_{critic,\,collapse}$ *(years): ASTM A-106 Gr. A* = 8.98*: ASTM A-106 Gr. B* = 8.16*; API-A* = 8.08	ASTM A-106 Gr. A> ASTM A-106 Gr. B> API B
Fitness for service index (*FFS*ᵢ)	Max (FFS_i)	FFS_i *(ASTM A-106 Gr. A)* = 3.35 FFS_i *(ASTM A-106 Gr. B, API-B)*= 3.06	ASTM A-106> ASTM A-106 Gr. B = API-B

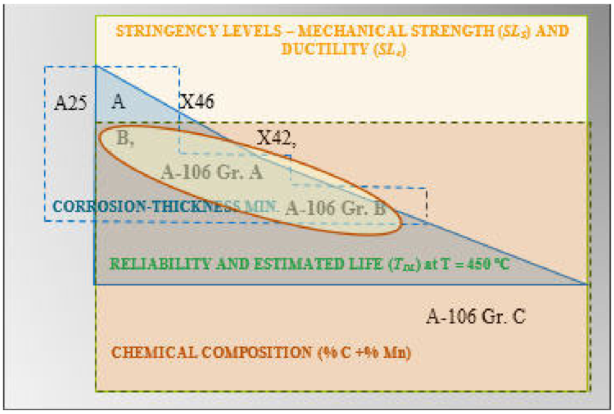

FIGURE 14. Diagram of selection according to the exclusion and selection criteria defined in Tables 15 and 16.

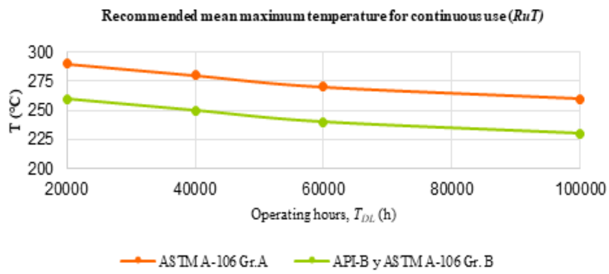

FIGURE 15. Determination of the maximum recommended operating temperature for continuous use (*RuT*) according to an analysis of parameters obtained according to API STD 530.

criteria used in the analysis in this work (evaluation according to stringency levels, assessment of the susceptibility to loss of integrity due to corrosion, chemical composition restrictions and evaluation of the reliability and estimated life at high temperature). Thus, a selection is made based on the fulfillment of all criteria.

As Fig. 14 shows, the materials that meet the criteria for exclusion are the following: ASTM A-106 Gr. A and B and API-B. After obtaining the best alternatives, an assessment of the restrictions recommended by continuous use is performed. The maximum recommended continuous use temperature (*RuT*) is calculated (Fig. 15) by setting the maximum temperature (*CET*) for which $\sigma_{col} > \sigma_{U,max}$ according to API STD 530 [29]. Thus, a long-term reliability analysis based on corrosion and high-temperature performance is conducted [35].

To avoid degradation of the mechanical properties at high temperature and to obtain a higher durability for 100,000 h, the temperature should be limited to 260 °C for ASTM A-106 Gr. A and 230 °C for API-B and ASTM A-106 Gr. B.

Finally, Table 17 summarizes the order of selection of materials with use limitations depending on the temperature and considering the effects of corrosion damage and possible overstress.

TABLE 17. Order of selection for the best alternative material with use limitations depending on the temperature and considering the effects of corrosion damage and possible overload.

Order of Selection	Materials	Limitations of use	
		RuT **(°C), for 100,000 h**	***T_{DLT} (years) at T = 450 °C***
1°	ASTM A-106 Gr. A	260	11.42
2°	ASTM A-106 Gr. B	230	6.85
3°	API-B	230	6.85

IV. CONCLUSIONS

In the new methodology developed in this work, several new elements have been incorporated, such as the concept of the suitability matrix and the fitness for service index (FFS_i), allowing a multiperspective approach to find the optimal solution to arduous material selection tasks in the petrochemical industry.

The approach allows a decision diagram to be built and establishes an order of selection along with several limitations of service in accordance with the maximum hours of operation of the component.

API materials A and B as well as materials ASTM A-106 Gr. A and Gr. B have higher reliability and suitability for service regarding the degradation mechanisms discussed in addition to an adequate balance between mechanical properties (mechanical strength and ductility).

However, considering the restrictions extracted from the analysis, the selected materials are API-B, ASTM A-106 Gr A and Gr. B since the API-A material would not meet the constraint (no. 2) that imposes a limit for the maximum carbon and manganese content (to maintain a balance between strength and ductility associated with the influence of the chemical composition on mechanical properties).

The maximum use limitations for the chosen materials are as follows: a critical exposure temperature (*CET*) equal to 450 °C for the material ASTM A-106 Gr. A and 440 °C for both API-B and ASTM A-106 Gr. B. On the other hand, maximum continuous use temperature (*RuT*) values have been established as 260 °C for ASTM A-106 Gr. A and 230 °C for API-B and ASTM A-106 Gr. B.

In the future, this new development can be applied as a decision algorithm within a framework of analysis based on the massive data collection obtained using sensor-based technologies (*IoT*), allowing the reliability of equipment and systems in the petrochemical sector to be improved.

LIST OF SYMBOLS AND ABBREVIATIONS

API	American Petroleum Institute
ASTM	American Society for Testing and Materials
e	Maximum elongation at fracture (%)
CET	Critical exposure temperature for an operation time - according to design – of at least 100,000 h
D	Ductility

IoT	Internet of Things
FFS	Fitness for service
FFS_i	Fitness for service index
L_e	Value of the requirement to analyze from the set {API, ASTM}
$L_{e,min}$	Minimum value from the set {API, ASTM}
MS	Mechanical strength
P	Design pressure
POF	Probability of failure
$POF_{corr+overload}$	Probability of failure due to corrosion and overload
POF_{T^a}	Probability of failure due to degradation of the material at high temperature
POF_{total}	Probability of failure due to corrosion and overload and high-temperature degradation
R	Reliability of the analyzed material with respect to the application
R_d	Inner radius (R_i) plus half the thickness (t). Typically, this is applied in piping and pressure vessel calculations using membrane stress theory.
R	corr Corrosion rate during the first year of exposure
RuT	Recommended mean temperature for continuous use
Δt	Thickness loss
SF	Safety factor for each material depending on the mechanical stresses applied
SL	Stringency level
SL_{max}	Maximum stringency level in the scale defined (5 points)
SL_s	Stringency level for strength properties
SL_e	Stringency level for ductility properties
t	Mean thickness
t_{min},	Minimum thickness to prevent plastic deformation
$t_{min,corr}$	Thickness after the loss due to corrosion
$t_{min,no\ collapse}$	Thickness limit before collapse
$T_{\text{critic,collapse}}$	Time to collapse after plastic deformation begins
T_{DL}	Expected operating lifetime determined by design (considering degradation at high temperature)
$T_{DL\ T^a}$	Expected operating lifetime determined by design at 450 °C
T_{max}	Maximum operation time (depending on the mechanisms of degradation)
V_{corr}	Corrosion rate after the first year of exposure
σ_{col}	Maximum effort allowed before collapse
$\sigma_{\text{t},corr}$	Maximum membrane stress after loss of thickness due to corrosion
$\sigma_{Y\ API\ 530}$	Maximum elastic stress at a temperature T according to API STD 530
$\sigma_{Y\ API\ 530,80}$	Maximum elastic stress at 80 °C according to API STD 530
φ	Outer diameter of pipe
σ_U	Ultimate tensile strength
$\sigma_{U,max}$	Maximum allowable rupture stress
σ_Y	Yield point
$\sigma_{Y\ max}$	Maximum elastic allowable stress (to prevent plastic deformation)

ACKNOWLEDGMENT

The authors would like to thank the UNED Research Group: Industrial Production and Manufacturing Engineering (IPME). This work is part of the activities included in the transfer contract of research results with reference 2019-CTINV-0068 (based on Article 83 of the Spanish Universities Act, 2007) between UNED and SGS TECNOS, being the scope aligned with the 9th Sustainable Development Goal related to *"Industry, Innovation and Infrastructure"*, as established by United Nations and included by the Spanish Government in the "Agenda 2030."

REFERENCES

[1] X. Song, Z. Zhai, P. Zhu, and J. Han, "A stochastic computational approach for the analysis of fuzzy systems," *IEEE Access*, vol. 5, pp. 13465–13477, 2017.

[2] A. Rodriguez-Prieto, A. M. Camacho, A. M. Aragon, M. A. Sebastian, and A. Yanguas-Gil, "Polymers selection for harsh environments to be processed using additive manufacturing techniques," *IEEE Access*, vol. 6, pp. 29899–29911, 2018.

[3] Y. Deng, L. Qiao, J. Zhu, and B. Yang, "Mechanical performance and microstructure prediction of hypereutectoid rail steels based on BP neural networks," *IEEE Access*, vol. 8, pp. 41905–41912, 2020.

[4] X. Xu and Q. Hua, "Industrial big data analysis in smart factory: Current status and research strategies," *IEEE Access*, vol. 5, pp. 17543–17551, 2017.

[5] F. Larrinaga, I. Aldalur, M. Illarramendi, M. Ituerbe, T. Pérez, G. Unamuno, C. Salvidea, and I. Lazkanoiturburu, "Analysis of technological architectures for the new industry paradigm 4.0," *Dyna*, vol. 94, no. 3, pp. 267–271, May 2019.

[6] D. Taco, D. Gutierrez, A. Castillo, and J. Iniguez, "Determining the optimal number of iterations for simulations by Monte Carlo method," *Dyna*, vol. 94, no. 2, pp. 129–130, Mar. 2019.

[7] D. Checa, J. Zulaykha, I. Lazkanotegi, and A. Bustillo, "Optimizing the machining of large castings by remote monitoring and 3D visualization," *Dyna*, vol. 93, no. 6, pp. 668–674, Nov. 2018.

[8] C. Martin and M. A. Parron, "Non-destructive testing techniques applied to inspection torches," *Dyna*, vol. 88, p. 1, Sep. 2013.

[9] M. A. Veganzones, "The challenges of the machine learning in the era of the big data," *Dyna*, vol. 94, no. 5, pp. 478–479, Sep. 2019.

[10] D. S. Bulgarevich, S. Tsukamoto, T. Kasuya, M. Demura, and M. Watanabe, "Pattern recognition with machine learning on optical microscopy images of typical metallurgical microstructures," *Sci. Rep.*, vol. 8, no. 1, p. 2078, Dec. 2018.

[11] C. Fragassa, M. Babic, C. P. Bergmann, and G. Minak, "Predicting the tensile behaviour of cast alloys by a pattern recognition analysis on experimental data," *Metals*, vol. 9, no. 5, p. 557, 2019.

[12] E. A. Ruelas, J. A. Vazquez, R. Baeza, J. A. Jimenez, M. Tapia, and V. Figueroa, "Pattern recognition and evaluation of the damage generated in low alloy steels from the digital image processing and artificial intelligence," *Dyna*, vol. 94, no. 4, p. 357, Jul. 2019.

[13] G. das Neves Carneiro and C. C. António, "Robustness and reliability of composite structures: Effects of different sources of uncertainty," *Int. J. Mech. Mater. Design*, vol. 15, no. 1, pp. 93–107, Mar. 2019.

[14] Y. Shi and Z. Lu, "Dynamic reliability analysis model for structure with both random and interval uncertainties," *Int. J. Mech. Mater. Design*, vol. 15, no. 3, pp. 521–537, Sep. 2019.
[15] C. Jiang, X. P. Huang, X. P. Wei, and N. Y. Liu, "A time-variant reliability analysis method for structural systems based on stochastic process discretization," *Int. J. Mech. Mater. Design*, vol. 13, no. 2, pp. 173–193, Jun. 2017.
[16] A. S. Milani and A. Shanian, "Gear material selection with uncertain and incomplete data. Material performance indices and decision aid model," *Int. J. Mech. Mater. Design*, vol. 3, no. 3, pp. 209–222, Sep. 2006.
[17] M. S. Attia, M. M. Megahed, M. A. Darwish, and S. Sundram, "Assessment of corrosion damage acceptance criteria in API579-ASME/1 code," *Int. J. Mech. Mater. Des.*, vol. 12, pp. 141–151, Mar. 2016.
[18] *Specification for Line Pipe*, American Petroleum Institute, Washington, DC, USA, 2018.
[19] *Standard Specification for Seamless Carbon Steel Pipe for High-Temperature Service*, American Society for Testing and Materials, West Conshohocken, PA, USA, 2019.
[20] M. Sharifian, M. Sharifian, and M. Sharifian, "Nonlinear elastoplastic analysis of pressure sensitive materials," *Int. J. Mech. Mater. Design*, vol. 14, no. 3, pp. 329–344, Sep. 2018.
[21] A. Rodríguez-Prieto, A. M. Camacho, and M. A. Sebastián, "Multicriteria materials selection for extreme operating conditions based on a multiobjective analysis of irradiation embrittlement and hot cracking prediction models," *Int. J. Mech. Mater. Design*, vol. 14, no. 4, pp. 617–634, Dec. 2018.
[22] M. Yan, B. Sun, B. Liao, Y. Ren, J. Yao, and M. Wei, "FORM and out-crossing combined time-variant reliability analysis method for ship structures," *IEEE Access*, vol. 6, pp. 9723–9732, 2018.
[23] V. T. Malcolm, "Creep resistant noncorrosive steel," U.S. Patent. 1 915 065 A, Jun. 20, 1933.
[24] Á. Rodríguez-Prieto, A. M. Camacho, and M. Á. Sebastián, "Materials selection criteria for nuclear power applications: A decision algorithm," *JOM*, vol. 68, no. 2, pp. 496–506, Feb. 2016.
[25] *Risk-Based Inspection Technology*, American Petroleum Institute, Washington, DC, USA, 2016.
[26] *Corrosion of Metals and Alloys—Corrosivity of Atmospheres—Classification, Determination and Estimation*, International Standardization Organization, Geneva, Switzerland, 2012.
[27] *Corrosion of Metals and Alloys—Corrosivity of Atmospheres—Guiding Values for the Corrosivity Categories*, International Standardization Organization, Geneva, Switzerland, 2012.
[28] *Piping Inspection Code: In-Service Inspection, Rating, Repair, and Alteration of Piping Systems*, American Petroleum Institute, Washington, DC, USA:, 2017.
[29] *Calculation of Heater-tube Thickness in Petroleum Refineries*, American Petroleum Institute, Washington, DC, USA, 2015.
[30] A. Coro, M. Abasolo, J. Aguirrebeitia, and L. López De Lacalle, "Inspection scheduling based on reliability updating of gas turbine welded structures," *Adv. Mech. Eng.*, vol. 11, no. 1, Jan. 2019, Art. no. 168781401881928.
[31] A. Coro, L. M. Macareno, J. Aguirrebeitia, and L. N. López De Lacalle, "A methodology to evaluate the reliability impact of the replacement of welded components by additive manufacturing spare parts," *Metals*, vol. 9, no. 9, p. 932, 2019.
[32] D. M. Krahmer, R. Polvorosa, L. N. López De Lacalle, U. Alonso-Pinillos, G. Abate, and F. Riu, "Alternatives for specimen manufacturing in tensile testing of steel plates," *Experim. Techn.*, vol. 40, no. 6, pp. 1555–1565, Dec. 2016.
[33] E. Zio, "Reliability engineering: Old problems and new challenges," *Rel. Eng. Syst. Saf.*, vol. 94, no. 2, pp. 125–141, Feb. 2009.
[34] W. Liu, Z. Song, Z. Wan, and J. Li, "Lifecycle operational reliability assessment of water distribution networks based on the probability density evolution method," *Probabilistic Eng. Mech.*, vol. 59, Jan. 2020, Art. no. 103037.
[35] X. Han, D. Y. Yang, and D. M. Frangopol, "Time-variant reliability analysis of steel plates in marine environments considering pit nucleation and propagation," *Probabilistic Eng. Mech.*, vol. 57, pp. 32–42, Jul. 2019.

ALVARO RODRÍGUEZ-PRIETO received the M.Sc. degree in materials engineering from the Complutense University of Madrid (UCM), in 2007, and the M.Sc. and Ph.D. degrees in advanced manufacturing engineering from National Distance Education University (UNED), in 2011 and 2014, respectively. He has been a Senior Engineer and Project Manager with SGS Tecnos, since 2007. He is currently an Assistant Professor with the Department of Manufacturing Engineering, UNED, Spain. His major current research interest includes innovation in materials selection methodologies and materials performance evaluation for demanding applications.

ANA MARÍA CAMACHO received the M.Sc. degree in industrial engineering from the University of Castilla-La Mancha (UCLM), in 2001, and the Ph.D. degree in industrial engineering from the National Distance Education University (UNED), Spain, in 2005. She is currently a Professor with the Department of Manufacturing Engineering, UNED. Her main research interest is the innovation in manufacturing engineering and materials technology, especially focused in analysis of metal forming and additive manufacturing techniques through computer aided engineering tools and experimental testing, and the development of methodologies for materials selection in demanding applications.

MANUEL CALLEJAS received the M.Sc. degree in materials and metallurgical engineering from the Complutense University of Madrid (UCM), in 1988. He has been working in materials science and metallurgical engineering for over 25 years, participating in numerous industrial projects as the Manager and an Assessor of materials technology discipline, including materials performance and forensic engineering analyses mainly for petrochemical and oil and gas industries. He is currently the Manager of industrial inspection and the Technical Assistance with SGS Spain.

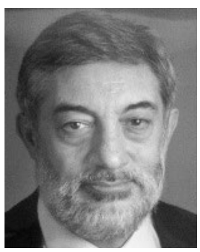

MIGUEL A. SEBASTIÁN received the M.Sc. degree in industrial engineering and the Ph.D. degree from the Technical University of Madrid (UPM), in 1976 and 1980, respectively. He has authored numerous works and scientific-technical articles in the areas of production and manufacturing engineering. He has participated in Research Projects supported by the Department of Science and Innovation of Spanish Government. He is currently a Full Professor with National Distance Education University (UNED), Spain.